Atmos. Chem. Phys. Discuss., 11, 14883–14902, 2011
www.atmos-chem-phys-discuss.net/11/14883/2011/
doi:10.5194/acpd-11-14883-2011

Atmospheric Chemistry and Physics Discussions

Revised identification of tropical oceanic cumulus congestus as viewed by CloudSat

S. P. F. Casey[1,*], **E. J. Fetzer**[1], **and B. H. Kahn**[1]

[1]Jet Propulsion Laboratory, Pasadena, CA, USA
[*]current address: Earth System Science Interdisciplinary Center/Joint Center for Satellite Data Assimilation, College Park, MD, USA

Received: 25 January 2011 – Accepted: 6 May 2011 – Published: 17 May 2011

Correspondence to: S. P. F. Casey (sean.casey@noaa.gov.)

Published by Copernicus Publications on behalf of the European Geosciences Union.

Abstract

Congestus cloud convective features are examined in one year of tropical oceanic cloud observations from the CloudSat/CALIPSO instruments. Two types of convective clouds (cumulus and deep convective, based on classification profiles from radar), and associated differences in radar reflectivity and radar/lidar cloud-top height are considered. Congestus convective features are defined as contiguous convective clouds with heights between 3 and 9 km. A majority of congestus convective features satisfy one of three criteria used in previous studies: (1) CloudSat and CALIPSO cloud-top heights less than 1 km apart; (2) CloudSat 0 dBZ echo-top height less than 1 km from CloudSat cloud-top height, and (3) CloudSat 10 dBZ echo-top height less than 2 km from CloudSat cloud-top height. However, less than half of congestus convective features satisfy all three of these requirements. This implies that previous methods used to identify congestus clouds may be biased towards more vigorous convection, missing more than half of observed congestus and significantly misrepresenting the deduced relationship between congestus clouds and their surroundings.

1 Introduction

Johnson et al. (1999) noted that tropical oceanic convective clouds can be grouped into three categories: shallow cumulus, with cloud-top heights near the trade inversion 1–2 km above the surface; mid-level cumulus congestus clouds, with cloud tops near the 0 °C melting level; and deep cumulonimbus clouds, with cloud-tops near the tropopause. While shallow and deep convective have long been acknowledged, the role of mid-level cumulus congestus has only recently become recognized. Kikuchi and Takayabu (2004) identified the cloud types with different stages of the Madden-Julian Oscillation (MJO) as (1) a "suppressed stage" with few clouds; (2) a "shallow convective stage" with shallow clouds; (3) a "developing stage" with cumulus congestus clouds; (4) a "mature stage" with deep convective clouds; and (5) a "decaying stage" with anvil

ACPD
11, 14883–14902, 2011

clouds. Similarly, Mapes et al. (2006), Chen and Del Genio (2009) and Tromeur and Rossow (2010) noted increased occurrence of congestus clouds prior to peak rainfall events associated with deep convection. Despite the observational evidence of congestus clouds, however, they were not accurately reproduced in global circulation model parameterizations until recently (Khouider and Majda, 2006; Sherwood et al., 2010).

The spatial coverage of satellites allows for identification of characteristics of congestus clouds globally. The twice-daily low-earth orbit satellite observations, as from CloudSat and Cloud-Aerosol Lidar and Infrared Pathfinder Satellite Observation (CALIPSO) (Stephens et al., 2008; Winker et al., 2009) can provide fine spatial resolution measurements of congestus cloud features despite the limitations of analyzing convective life-cycle (Luo et al., 2009). Automated methods for identifying congestus would simplify understanding regional differences in congestus populations, connections to surface and environmental conditions, and applications to tropical climatology and many other important areas of research. Methods for identifying congestus, however, have varied (Rossow et al., 2005).

Recently, Luo et al. (2009) have identified congestus using reflectivity and cloud-height information from CloudSat and CALIPSO. Congestus observations were defined as clouds with cloud-top heights (CTH) between 3 and 9 km (Jensen and Del Genio, 2006) and with continuous radar echo from CTH to near the ground which satisfy three criteria: (1) difference between CloudSat and CALIPSO CTH of less than 1 km, (2) difference between CloudSat CTH and 0 dBZ echo-top height (ETH) of less than 1 km, and (3) difference between CloudSat and 10 dBZ ETH of less than 2 km. These values were identified in Luo et al. (2008) as cloud and echo characteristics shared by a majority of deep convective clouds. Luo et al. (2009) also included a method for determining the convective buoyancy of CloudSat-viewed convection; this approach is useful for determining whether an observed convective cloud is "terminal", remaining at congestus heights, or "transient", rising to become deep convection. However, this method has not been verified with independent observations, and as such this paper

ACPD
11, 14883–14902, 2011

will not include this method at this time.

This study relates the CloudSat-provided cloud classification data to radar and lidar characteristics of mid-level tropical oceanic convection. We then compare these statistics to those utilized by Luo et al. (2009), and assess how well the Luo et al. (2009) criteria capture congestus.

2 Methodology

Clouds are identified using data measured in 2008 (full year) from two A-Train satellite instruments. The Cloud Profiling Radar (CPR) onboard CloudSat (Stephens et al., 2008) transmits at 94-GHz (W-band) and has a minimum detectable reflectivity of −28 dBZ. It is a nadir-viewing instrument with an effective horizontal resolution of 1.4 km. Three data products provided by the CloudSat science team will be used. First, the main 2B-GEOPROF (Marchand et al., 2008) product gives cloud mask/certainty information as well as radar reflectivity values. Next, the 2B-GEOPROF-LIDAR product (Mace et al., 2009) combines CPR data with measurements from the Cloud-Aerosol Lidar with Orthogonal Polarization (CALIOP) lidar onboard CALIPSO. This product interpolates CALIPSO high-resolution data onto the CloudSat footprint. As CALIPSO passes over the same location 15 s after CloudSat, the measurements can be assumed to be simultaneous.

Finally, the cloud classification (2B-CLDCLASS) product will be used. Two types of convection are identified using the 2B-CLDCLASS algorithm (Sassen and Wang, 2008); a "cumulus" flag that identifies areas of low- to medium-level convection, and a "deep convection" flag that identifies convective cells with cold cloud-tops ($T < 258$ K) using reanalysis temperatures. As we are interested in tropical oceanic regions, we limit our study to areas between 15° S and 15° N labelled as ocean by the CLDCLASS product.

Congestus clouds are defined here by two criteria. First is a cloud-top height (CTH) between 3 and 9 km, utilized in Jensen and Del Genio (2006). We impose a second

ACPD
11, 14883–14902, 2011

requirement of cloud base to be within 1 km of the surface; this ensures the cloud in question is related to surface-driven processes while taking into account the ground clutter issues in the lowest 1 km of CloudSat data (Tanelli et al., 2009). Three levels of radar-detected CTH are considered, based on the degree of certainty of cloud detection in the 2B-GEOPROF product: cloud mask = 40 marks the most certain cloud detection, while cloud masks 30 and 20 mark decreasing areas of certainty. As CloudSat measurements are reported on a distance vs. height grid, these three CTH values are calculated from the reported 2-dimensional cloud-mask grid (more information in Marchand et al., 2008). A fourth CTH, as identified in the GEOPROF-Lidar product as being observed by CALIPSO, is also considered. In addition, two levels of radar-reflectivity echo top height (ETH) are identified: 0 and 10 dBZ. As mentioned in the introduction, these values were noted in Luo et al. (2008), and applied in Luo et al. (2009) to identify congestus clouds.

3 Results

Analyses of the convective echo characteristics are grouped in three sections. The first looks at statistics compiled from single CloudSat fields-of-view; this allows for profile-specific comparisons. The second section looks at coherent convective features along the CloudSat path; here identification focuses on the characteristics of specific cloud types. Finally, we will look at the applicability of the mean statistics obtained here for identifying congestus, similar to Luo et al. (2009)'s application of the Luo et al. (2008) means.

3.1 Field-of-view analysis

Figure 1 shows the relative frequency of convective CTH, separated by cloud classification and cloud mask. A vertical delineation between the two cloud types is apparent; the peak for the three cumulus curves lies around 4 km, while the deep convection

ACPD
11, 14883–14902, 2011

peaks lie near 14–15 km. Cloud class does not uniquely distinguish deep and shallow clouds, however. Some clouds flagged as deep convection are seen to have CTH heights of 2–3 km above the surface. In addition, a weak cumulus-20 peak is noted at 14 km; no such peak is noted in cumulus-30, suggesting some are cases where the difference in height between cumulus-20 and cumulus-30 may exceed 5 km. Only slight differences are noted between cloud masks 30 and 40; the curves for cumulus-30 and cumulus-40 are nearly indistinguishable.

Table 1 lists CTH and ETH differences for congestus (CTH of 3 to 9 km and radar cloud base below 1 km), separated by the six cloud classification/mask categories. The third column lists the number of fields-of-view. More congestus fields-of-view are identified as cumulus by the 2B-CLDCLASS algorithm than as deep convection, at a rate of nearly two to one. Also, more cumulus-20 are identified as congestus than cumulus-40; this suggests a situation where the cumulus-20 CTH is greater than 3 km while cumulus-40 is below 3 km, or, a cumulus-20 cloud has no areas reporting a cloud mask of 40. Conversely, more deep convection-40 are identified as congestus than deep convection-20; this may be due to a deep convection-20 CTH greater than 9 km and deep convection-40 CTH less than 9 km (and thus identified as congestus here).

The fourth column of Table 1 lists the mean difference between CALIPSO and CloudSat CTH. Because the CALIPSO lidar is more sensitive to smaller particles than is the CloudSat radar, CTH is expected to be higher from CALIPSO. The mean CTH difference ranges from 2.7 to 5.8 km in Table 1. As expected, the mean CTH difference between CALIPSO and radar cloud mask 20 CTH is higher than between CALIPSO and radar cloud mask 40 CTH. The distance is also smaller above pixels identified as deep convection than pixels identified as cumulus. Column 4 also lists the percentage of cases with the appropriate cloud mask/classification where CALIPSO identifies a higher cloud top than CloudSat. This occurs for about 75 % of cumulus cases and 90 % of deep convective cases. The CALIPSO lidar beam is extinguished at an optical depth of about 3, so the cases where a CALIPSO CTH is not identified concurrent with a CloudSat CTH may be due to the CALIPSO beam being extinguished by a non-

ACPD
11, 14883–14902, 2011

connected cloud higher in the atmosphere. The averaging of smaller CALIPSO pixels onto the CloudSat footprint may also contribute to pixels where CALIPSO reports a CTH below that observed by CloudSat.

The fifth column of Table 1 lists the difference between CloudSat CTH and 0 dBZ ETH. The percentage values in this column show that a majority of convective pixels for both cloud types contain a 0 dBZ echo within the cloud. This height difference ranges from 900–1700 m, with higher cloud mask values of CTH located nearer the 0 dBZ ETH than lower values. The 0 dBZ ETH is on average closer to cumulus CTH than to deep convective CTH, though this difference is slight. The final column is similar to column 5, except shows results for the 10 dBZ ETH. As with 0 dBZ ETH, the 10 dBZ ETH is closer to the cumulus CTH than to deep convection CTH. The mean height difference is around 1600 m for cumulus-identified pixels, and around 2500 m for deep-convection-identified pixels. This is greater than for the 0 dBZ ETH. However, less than half of cumulus-identified fields-of-view contain reflectivities greater than 10 dBZ, while slightly more than half of deep-convection-identified fields-of-view do. This may reveal the extent of the edges of convective clouds seen by CloudSat; non-precipitating edges of convective features would return smaller echoes.

These results summarize an instantaneous field-of-view perspective of congestus clouds. We now turn to a convective-feature analysis of the CloudSat cloud classification and mask.

3.2 Convective feature analysis

Here we define "convective feature" as a continuous swath of fields-of-view along the CloudSat path for which the cloud class is identified as either cumulus or deep convective. This definition does not distinguish individual convective cells; if two or more cells are located next to each other, this classification treats them as one continuous convective feature. An example of a convective feature can be seen in Fig. 2, which shows the returned radar power (top panel) and associated 2B-CLDCLASS classifications (bottom panel) for a sample scan (orbit 2680, section 31) over the

ACPD
11, 14883–14902, 2011

Pacific Ocean (http://www.cloudsat.cira.colostate.edu/dpcstatusQL.php). Though multiple narrow cells can be identified in the top panel, the cloud classification groups these all together into one cumulus feature (identified in orange on the bottom panel). The highest CTH among all the profiles in one convective feature is considered the convective feature's CTH.

Figure 3 shows the regional distribution of convective features identified using the CTH criteria described above. They seem to mirror the expected convective distribution in the tropics (Yanai et al., 1973), with the exception of fewer congestus convective features noted over the West Pacific/maritime continent warm pool region. The lower amounts of congestus in this region are also reported in Rossow et al. (2005). Sassen and Wong (2008) also confirm a relative Maritime Continent void in both cumulus and deep convective clouds using one year of data.

Table 2 lists ETH difference for congestus convective features, separated by the same six cloud classification/mask categories used to characterize individual fields-of-view in Table 1. Only convective features made up entirely of cumulus- or deep-convective-identified pixels are included in Table 2, to allow for comparison of the two cloud type identifications; about 20 % of the total convective features identified are made up of a combination of cumulus and deep-convective pixels. As before, more features are identified as cumulus than as deep convection. Dividing column 3 in Table 1 by column 3 in Table 2, it is clear that the ratio of cumulus fields-of-view to cumulus-convective features (6 to 1) is less than the ratio of deep convective fields-of-view to deep-convective features (17 to 1). This is because deep convective features are larger horizontally than shallower cumulus features (Johnson et al., 1999).

According to Table 2, almost all deep convective features are associated with a CTH observed by CALIPSO (99 %); the number is slightly lower for cumulus features. This is to be expected since a cumulus feature, being closer to the ground, would have more space between it and the tropopause than a deep convective feature, and thus more room for another cloud such as thin cirrus or anvil clouds detectable by CALIPSO. The difference in height between CloudSat and CALIPSO is lower than in Table 1: about

ACPD
11, 14883–14902, 2011

1–2 km for cumulus and 1 km for deep convection.

The distance between the top of the convective feature and the highest 0 dBZ height (column 5 in Table 2) is lower than for the single field-of-view comparison. This distance averages about 700 m for cumulus and 800 m for deep convection. More convective features contain 0 dBZ echoes than individual fields-of-view summarized in Table 1.

Finally, when comparing convective feature cloud height to 10 dBZ ETH, we see that more convective features than individual fields of view contain 10-dBZ echoes. Unlike for the fields-of-view analysis, a majority (55–60 %) of cumulus convective features contain a 10-dBZ echo; 75 % of deep convective features contain echoes greater than 10 dBZ. The average distance in CTH for cumulus-identified convection is about 1.2 km, and for deep convective features is about 1.7 km.

3.3 Quantitative identification of congestus

We now return to the three criteria used to identify congestus in Luo et al. (2009), as described in the introduction. Rather than comparing all three cloud-mask values, we will only use a cloud mask = 30 for this section, as this was the value used in the Luo et al. (2009) study. The mean values in Table 2 appear to corroborate the criteria values; the mean difference between CTH and 0 dBZ ETH is less than 1 km, and between CTH and 10 dBZ ETH is less than 2 km. The mean deep convective radar-lidar difference is slightly more than 1 km; however, the mean for cumulus-identified clouds is less than 1 km, and many more congestus clouds are identified as cumulus than as deep convective. However, for the Luo et al. (2009) identification method to be considered effective, there must be a majority of features that satisfy all three requirements.

Table 3 show information for features meeting these criteria. Appropriate statistics for convective features made up of a combination of cumulus and deep-convective fields of view are also included in this table. A majority of features satisfy at least one individual requirement. However, less than half (45 %) of features for each convective cloud type satisfy all three. The main limiting factor appears to be the 10 dBZ ETH threshold. Table 2 shows that only 60–75 % of contiguous convective features contain

ACPD
11, 14883–14902, 2011

a 10 dBZ ETH; only 55 % of convective features have a 10 dBZ ETH within 2 km of CloudSat CTH (Table 3). This suggests that an identification scheme based purely on thresholding on the mean feature values may miss over half of all observed congestus.

Figure 4 shows the regional distribution of convective features that satisfy the Luo et al. (2009) criteria. Blue and green colors mark areas where a majority of features satisfy the given criteria; purple and red mark where less than 50 % of features satisfy. Comparing Figs. 3 and 4, it is again clear that the 10 dBZ ETH threshold is the main limiting factor in determining the existence of congestus cloud; applying this criterion alone misses over 70 % of congestus convective features over parts of the maritime continent/West Pacific. (Near the islands of the Maritime Continent, the fraction of congestus satisfying each criterion appears to decrease; as this study looks at ocean-only scenes as identified in the 2B-CLDCLASS algorithm, no data is available over the larger islands in the Indonesian region, and this decrease should be considered an artifact.)

Also, more convective features fit any combination of criteria over the central Pacific than over the maritime continent/West Pacific in Fig. 4. Zonal differences are apparent, but no strong pattern appears over these regions in the meridional direction. On the other hand, zonal and meridional patterns are noted in the total count distributions in Fig. 3, corresponding to well-known areas of enhanced convection (Intertropical Convergence Zone, South Pacific Convergence Zone, etc.). Comparison of Figs. 3 and 4 suggests that congestus convective features meeting the convective criteria of Luo et al. (2009) may be related to a zonal phenomenon such as the Walker circulation. Further investigation is warranted to identify the large-scale dynamic features that could affect the strength of observed congestus in comparison with the Luo et al. (2009) method.

ACPD
11, 14883–14902, 2011

4 Summary and conclusions

This study describes characteristics of cloud- and echo-top height associated with tropical oceanic congestus clouds. In addition to checking three different cloud masks derived from the CloudSat GEOPROF product, we looked at the distance from CTH to CALIPSO CTH, 0 dBZ ETH, and 10 dBZ ETH. These three heights were used in Luo et al. (2008) to describe tall convective cells.

In a profile-by-profile analysis, a majority of cells of both cloud types contain a 0 dBZ echo; however, less than half of cumulus-identified fields-of-view have echoes greater than 10 dBZ. A majority of contiguous convective features contain a 10-dBZ echo. A majority of features also satisfy one of the three requirements for congestus clouds used in Luo et al. (2009).

When applying these criteria, however, only about 45 % of convective features satisfy all three requirements. Analyses of convective features using this identification would therefore be skewed toward the more vigorous congestus convection (i.e., higher radar reflectivities) rather than being representative of congestus as a whole. The criteria appear to do a better job of identifying congestus convection over the eastern and central Pacific than over the Western Pacific and Maritime Continent regions. This may relate to the role of subsidence in the Walker Circulation, capping strong cells that would otherwise rise to become deeper clouds (Sherwood et al., 2010).

This paper examines the conditions for applying the mean threshold statistics from Luo et al. (2008) to identify congestus. The applicability of the method, of course, depends on the phenomena of interest. The quantitative method from Luo et al. (2009) identifies strong congestus features; i.e., those with high (> 10 dBZ) reflectivity and small differences between CTH and ETH. These may be more useful in identifying transient congestus (mid-level convection rising to become a deeper cloud). Identification of congestus features in general may be better accomplished by the CLDCLASS algorithm of Sassen and Wang (2008), as well as using the 3 to 9 km height characteristics used in Jensen and Del Genio (2006) to separate congestus from shallow and

ACPD
11, 14883–14902, 2011

deep clouds. Together, these methods identify both weaker and stronger congestus convective features, yielding a larger set of congestus clouds for analysis.

Acknowledgement. The research described in this paper was carried out at the Jet Propulsion Laboratory, California Institute of Technology, under a contract with the National Aeronautics and Space Administration. It was supported by the NASA Making Earth Science Data Records for Use in Research Environments (MEaSUREs) project.

References

Chen, Y. and Del Genio, A. D.: Evaluation of tropical cloud regimes in observations and a general circulation model, Clim. Dynam., 32, 355–369, doi:10.1007/s00382-008-0386-6, 2009.

Jensen, M. P. and Del Genio, A. D.: Factors limiting convective cloud-top height at the ARM Nauru Island climate research facility, J. Climate, 19, 2105–2117, 2006.

Johnson, R. H., Richenbach, T. M., Rutledge, S. A., Ciesielski, P. E., and Schubert, W. H.: Trimodal characteristics of tropical convection, J. Climate, 12, 2397–2418, 1999.

Khouider, B. and Majda, A. J.: A simple multicloud parameterization for convectively coupled active waves. Part I. Linear analysis, J. Atmos. Sci., 63, 1308–1323, 2006.

Kikuchi, K. and Takayabu, Y. N.: The development of organized convection associated with the MJO during TOGA COARE IOP: trimodal characteristics, Geophys. Res. Lett., 31, 10, L10101, 2004.

Luo, Z. Z., Liu, G. Y., and Stephens, G. L.: CloudSat adding new insight into tropical penetrating convection, Geophys. Res. Lett., 35, L19819, doi:10.1029/2008GL035330, 2008.

Luo, Z. Z., Liu, G. Y., Stephens, G. L., and Johnson, R. H.: Terminal versus transient cumulus congestus: a CloudSat perspective, Geophys. Res. Lett., 36, L05808, 2009.

Mace, G. G., Zhang, Q., Vaughan, M., Marchand, R., Stephens, G., Trepte, C., and Winker, D.: A description of hydrometeor layer occurrence statistics derived from the first year of merged Cloudsat and CALIPSO data, J. Geophys. Res., 114, D00A26, doi:10.1029/2007JD009755, 2009.

Marchand, R. T., Mace, G. G., Ackerman, T., and Stephens, G.: Hydrometeor detection using CloudSat: an Earth-orbiting 94 GHz cloud radar, J. Atmos. Ocean. Tech., 25, 519–533, 2008.

ACPD

11, 14883–14902, 2011

Mapes, B., Tulich, S., Lin, J., and Zuidema, P.: The mesoscale convection life cycle: building block or prototypes for large-scale tropical waves?, Dynam. Atmos. Oceans, 42(1–4), 3–29, doi:10.1016/j.dynatmoce.2006.03.003, 2006.

Rossow, W. B., Tselioudis, G., Polak, A., and Jakob, C.: Tropical climate described as a distribution of weather states indicated by distinct mesoscale cloud property mixtures, Geophys. Res. Lett., 32, L21812, doi:10.1029/2005GL024584, 2005.

Sassen, K. and Wang, Z.: Classifying clouds around the globe with the CloudSat radar: 1-year of results, Geophys. Res. Lett., 35, L04805, doi:10.1029/2007GL032591, 2008.

Sherwood, S. C., Roca, R., Weckwerth, T. M., and Andronova, N. G.: Tropospheric water vapor, convection, and climate, Rev. Geophys., 48, RG2001, doi:10.1029/2009RG000301, 2010.

Stephens, G. L., Vane, D. G., Tanelli, S., Im, E., Durden, S., Rokey, M., Reinke, D., Partain, P., Mace, G. G., Austin, R., L'Ecuyer, T., Haynes, J., Lebsock, M., Suzuki, K., Waliser, D., Wu, D., Kay, J., and Gettelman, A.: CloudSat mission: performance and early science after the first year of operation, J. Geophys. Res., 113, D00A18, doi:10.1029/2008JD009982, 2008.

Tanelli, S., Durden, S. L., Im, E., Pak, K. S., Reinke, D. G., Partain, P., Haynes, J. M., and Marchand, R. T.: CloudSat's cloud profiling radar after two years in orbit: performance, calibration, and processing, IEEE T. Geosci. Remote, 46, 11, 2009.

Tromeur, E. and Rossow, W. B.: Interaction of the deep convection with the large scale circulation in the MJO, J. Climate, 23, 7, 1837–1853, 2010.

Winker, D. M., Vaughan, M. A., Omar, A., Hu, Y. X., Powell, K. A., Liu, Z. Y., Hunt, W. H., and Young, S. A.: Overview of the CALIPSO mission and CALIOP data processing algorithms, J. Atmos. Ocean. Tech., 26, 11, 2310–2323, 2009.

Yanai, M., Esbensen, S., and Chu, J. H.: Determination of bulk properties of tropical cloud clusters from large-scale heat and moisture budgets, J. Atmos. Sci., 30, 611–627.

ACPD
11, 14883–14902, 2011

Table 1. CALIPSO minus CloudSat CTH differences for individual congestus fields-of-view, and mean differences between CloudSat CTH and ETH, separated by the six cloud classification/mask categories. Column 4 also lists the percent of cases where CALIPSO identifies a higher cloud top than CloudSat; columns 5 and 6 list the percent of cases where a 0 or 10 dBZ echo, respectively, is identified.

Cloud classification	Cloud mask	Counts	ΔH (CALIPSO-CloudSat)	ΔH (0 dBZ)	ΔH (10 dBZ)
Cumulus	20	238014	5802.4 m (65.6 %)	1206.3 m (76.5 %)	1759.3 m (35.7 %)
	30	208895	3818.7 m (77.2 %)	1021.2 m (80.3 %)	1633.3 m (40.7 %)
	40	201336	3286.7 m (80.7 %)	966.7 m (81.2 %)	1592.7 m (41.7 %)
Deep convection	20	106205	3468.5 m (78.8 %)	1652.9 m (91.6 %)	2627.1 m (50.8 %)
	30	123050	2708.2 m (92.0 %)	1367.5 m (86.6 %)	2445.1 m (53.1 %)
	40	130192	2785.4 m (94.3 %)	1295.2 m (83.9 %)	2396.0 m (52.9 %)

ACPD
11, 14883–14902, 2011

Table 2. CTH and ETH differences for contiguous congestus convective features, separated by the six cloud classification/mask categories.

Cloud classification	Cloud mask	Counts	ΔH (CALIPSO-CloudSat)	ΔH (0 dBZ)	ΔH (10 dBZ)
Cumulus	20	38 175	2312.1 m (90.9 %)	796.0 m (77.4 %)	1308.0 m (52.0 %)
	30	32 758	841.7 m (99.6 %)	656.8 m (84.1 %)	1209.5 m (61.4 %)
	40	31 643	747.9 m (99.8 %)	615.7 m (85.2 %)	1176.4 m (63.0 %)
Deep convection	20	6288	1481.9 m (93.0 %)	1053.6 m (96.2 %)	1875.9 m (73.2 %)
	30	7476	1056.1 m (99.8 %)	844.4 m (94.3 %)	1731.2 m (76.0 %)
	40	8094	1175.0 m (99.9 %)	801.3 m (93.1 %)	1684.9 m (76.0 %)

ACPD
11, 14883–14902, 2011

Table 3. Number of cells that satisfy Luo et al. (2009) requirements.

Cloud type	Total	With lidar $\Delta H < 1$ km	With 0 dBZ $\Delta H < 1$ km	With 10 dBZ $\Delta H < 2$ km	All three requirements
Cumulus only	32 758	25 834 (78.9 %)	23 915 (73.0 %)	18 027 (55.0 %)	15 168 (46.3 %)
Deep convection only	7476	5785 (77.4 %)	5530 (74.0 %)	4042 (54.1 %)	3324 (44.5 %)
Combination cumulus/deep convection	9272	7059 (76.1 %)	6522 (70.3 %)	4752 (51.3 %)	3885 (41.9 %)
Total	49 506	38 678 (78.1 %)	35 967 (72.7 %)	26 821 (54.2 %)	22 377 (45.2 %)

ACPD
11, 14883–14902, 2011

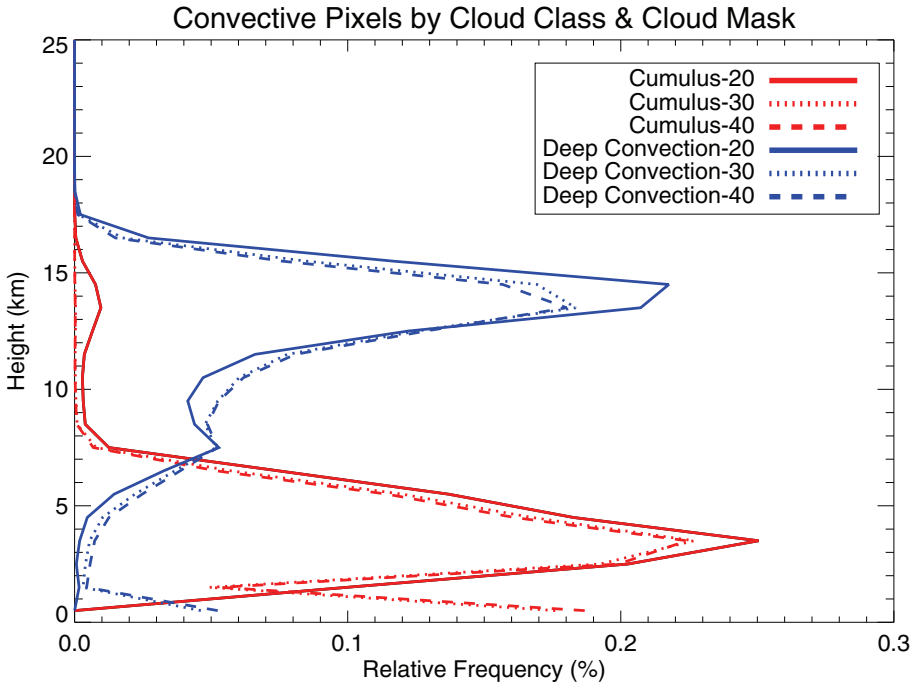

Fig. 1. Relative frequency of convective CTH, separated by cloud classification and radar mask cloud top height.

ACPD
11, 14883–14902, 2011

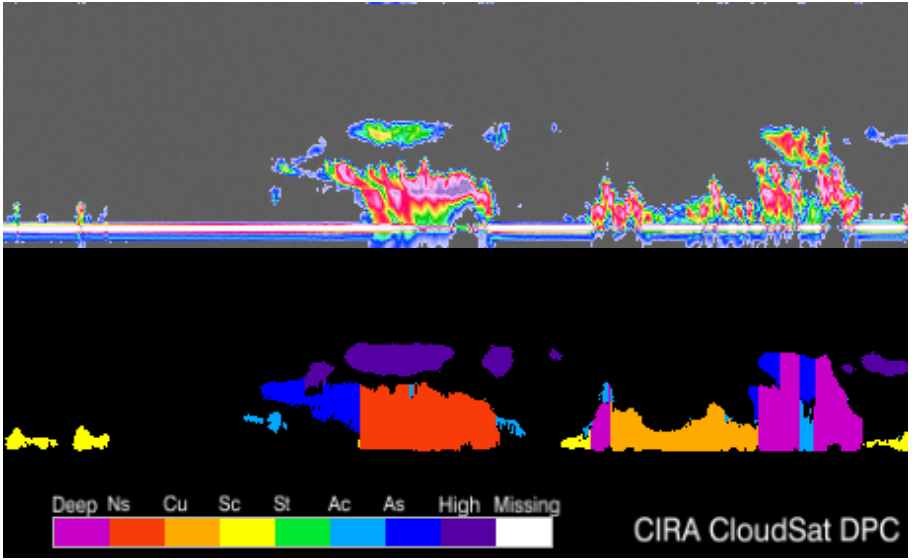

Fig. 2. Top: Sample returned power scan from CloudSat. Bottom: Associated 2B-CLDCLASS classification of the returned cells. Cu = cumulus, deep = deep convection. Both images taken from the CloudSat online quicklook archive: http://www.cloudsat.cira.colostate.edu/dpcstatusQL.php.

ACPD
11, 14883–14902, 2011

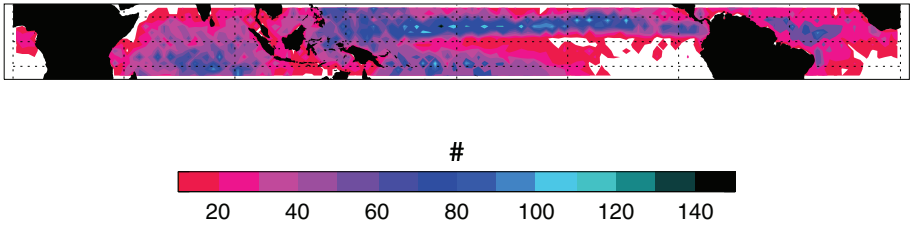

Fig. 3. Regional distribution of congestus convective features, contoured by the total number of observations over a 2.5° × 2.5° grid box. White areas mark regions where fewer than ten congestus convective features are observed.

ACPD
11, 14883–14902, 2011

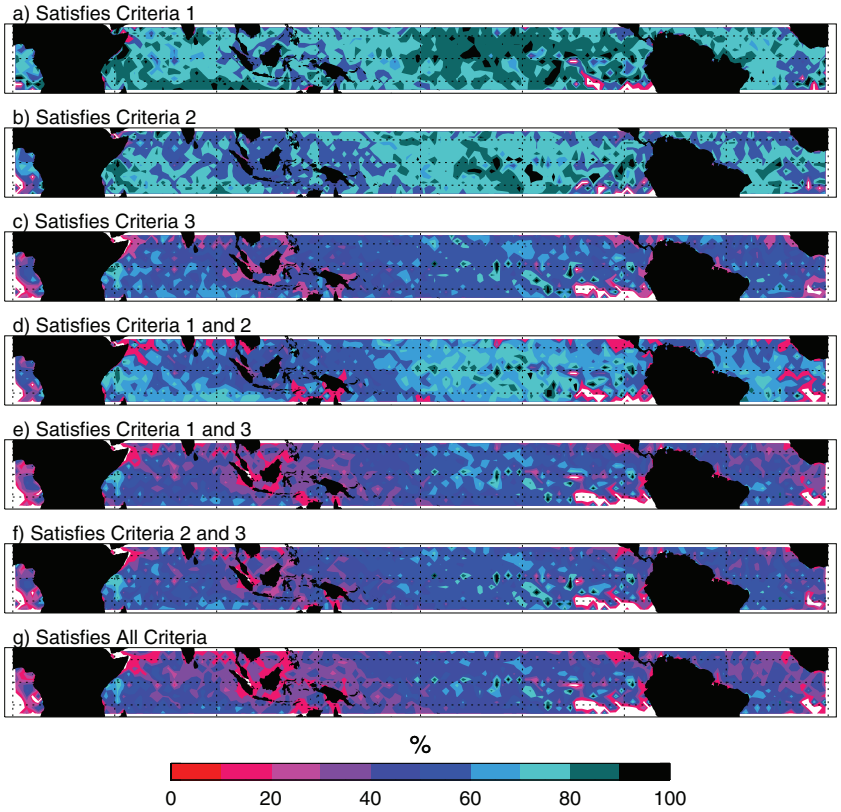

Fig. 4. Percentage of convective features in 2.5° longitude by 2.5° latitude boxes that satisfy the three Luo et al. (2009) criteria: (1) difference between CloudSat and CALIPSO CTH of less than 1 km, (2) difference between CloudSat CTH and 0 dBZ ETH of less than 1 km, and (3) difference between CloudSat and 10 dBZ ETH of less than 2 km. White areas mark regions where no congestus convective features are observed.

ACPD
11, 14883–14902, 2011